Biophysical *Journal*
Article

Biophysical Society

Adsorption of Phospholipids at the Air-Water Surface

Xuan Bai,[1,2,3] Lu Xu,[4] Jenny Y. Tang,[4] Yi Y. Zuo,[4,5,*] and Guoqing Hu[1,*]
[1]Department of Engineering Mechanics, Zhejiang University, Hangzhou, China; [2]The State Key Laboratory of Nonlinear Mechanics, Institute of Mechanics, Chinese Academy of Sciences, Beijing, China; [3]School of Engineering Science, University of Chinese Academy of Sciences, Beijing, China; [4]Department of Mechanical Engineering and [5]Department of Pediatrics, John A. Burns School of Medicine, University of Hawaii at Manoa, Honolulu, Hawaii

ABSTRACT Phospholipids are ubiquitous components of biomembranes and common biomaterials used in many bioengineering applications. Understanding adsorption of phospholipids at the air-water surface plays an important role in the study of pulmonary surfactants and cell membranes. To date, however, the biophysical mechanisms of phospholipid adsorption are still unknown. It is challenging to reveal the molecular structure of adsorbed phospholipid films. Using combined experiments with constrained drop surfactometry and molecular dynamics simulations, here, we studied the biophysical mechanisms of dipalmitoylphosphatidylcholine (DPPC) adsorption at the air-water surface. It was found that the DPPC film adsorbed from vesicles showed distinct equilibrium surface tensions from the DPPC monolayer spread via organic solvents. Our simulations revealed that only the outer leaflet of the DPPC vesicle is capable of unzipping and spreading at the air-water surface, whereas the inner leaflet remains intact and forms an inverted micelle to the interfacial monolayer. This inverted micelle increases the local curvature of the monolayer, thus leading to a loosely packed monolayer at the air-water surface and hence a higher equilibrium surface tension. These findings provide novel insights, to our knowledge, into the mechanism of the phospholipid and pulmonary surfactant adsorption and may help understand the structure-function correlation in biomembranes.

INTRODUCTION

Phospholipids, because of their amphipathic nature, self-assemble into vesicles once immersed in an aqueous environment (1,2). When lipid vesicles diffuse closely enough to a surface, they may adsorb to the surface, most likely driven by hydrophobic interactions (3–5). Understanding the adsorption process is of significance in various biological areas, such as membrane fusion and the formation of phospholipid-based interfacial films, for instance, pulmonary surfactant film, tear film, gut protective layer, and synovial articular junctions (6–11).

Adsorption of phospholipids at the air-water surface plays an important role in membrane fusion (12–15) and pulmonary surfactants (16–18). As the major component of pulmonary surfactant, phospholipids, especially dipalmitoylphosphatidylcholine (DPPC), are responsible for reducing the alveolar surface tension to very low values required for normal tidal breathing (8,19). DPPC is also the major component of most exogenous surfactants used to treat the neonatal respiratory distress syndrome (8,20).

Existing biophysical models suggest that during the adsorption process, lipid vesicles first diffuse from the bulk to the air-water surface, followed by subsequent unzipping and spreading at the surface (21,22). It is visualized that lipid vesicles in the bulk subphase are interrelated with the adsorbed film via stalk intermediate, thus allowing lipid exchange between vesicles and the adsorbed film (12,13). Adsorption is considered to reach an equilibrium when the lipid molecules are closely packed at the surface and reach a dynamic equilibrium with vesicles in the bulk phase (21,22).

Despite numerous experimental studies of lipid adsorption (22–26), the detailed biophysical mechanism of lipid vesicle adsorption is still unclear. Various experimental methodologies, including Langmuir balance (12), pulsating bubble surfactometry (27), captive bubble surfactometry (22), micropipette technique (28), and infrared reflection-absorption spectroscopy (25), have been used for measuring the dynamic surface tension and the structure of adsorbed phospholipid films. The dynamic surface tension measurements showed significant discrepancies with different preparations of DPPC vesicles (25,29,30). Many measured

Submitted May 8, 2019, and accepted for publication August 19, 2019.
*Correspondence: ghu@zju.edu.cn or yzuo@hawaii.edu
Xuan Bai and Lu Xu contributed equally to this work.
Editor: D. Peter Tieleman.
https://doi.org/10.1016/j.bpj.2019.08.022

equilibrium surface tensions were much higher than the theoretical equilibrium surface tension of the air-alkyl surface (21,24–26,28–31). Infrared reflection-absorption spectroscopy results showed that there were more than one monolayer at the air-water surface after adsorption of the DPPC vesicles (25,29,30). Abundant DPPC materials were found to be attached to the adsorbed interfacial monolayer, which were absent in a spread film (25,32).

Compared to experimental methods, coarse-grained MD (CGMD) simulations are advantageous in providing high-resolution molecular structures and dynamic details at the timescale over nanoseconds and, most importantly, at the length scale over tens of nanometers (33–37), comparable to the length scale of DPPC vesicles. CGMD simulations have succeeded in studying the structural transformation between the phospholipid monolayer at the air-water surface and the phospholipid bilayer in the subphase using the Martini force field (38,39). However, the original Martini force field underestimates the air-water surface tension, thus resulting in an unphysical adsorption behavior at the clean air-water surface.

Here, we used combined experimental methods and CGMD simulations to investigate the mechanism of lipid vesicle adsorption. We first used constrained drop surfactometry (CDS) (40) to determine the dynamic surface tension of various DPPC preparations. We then used the atomic force microscopy (AFM) to determine the micromorphology of the adsorbed DPPC film. Finally, we used CGMD simulations, based on a modified Martini force field, to simulate the adsorption process of various DPPC nanoassemblies (i.e., micelle, bilayer, and vesicle). We found that the adsorbed film from vesicles exhibited a much higher surface tension than the adsorbed films from bilayers and micelles. These surface tension differences were explained by differences in the molecular structure of the adsorbed films at the air-water surface.

MATERIALS AND METHODS

Preparation of DPPC vesicles

50 mg DPPC (Avanti Polar Lipids, Alabaster, AL) was dissolved in 2 mL chloroform to form a 25 mg/mL stock suspension. The organic solvent was evaporated under a nitrogen steam to deposit a thin lipid film on the wall of the glass vial. The deposited DPPC film was then hydrated with 5 mL phosphate-buffered saline (PBS) solution (121.5 mM NaCl, 25.2 mM Na_2HPO_4, and 4.8 mM KH_2PO_4 (pH 7.4)) and sonicated for 10 min. The suspension was then incubated for 3 h at 46°C (i.e., 5°C above the gel-to-liquid crystalline phase transition temperature of fully hydrated DPPC bilayers) (41). The DPPC vesicles were sonicated using an ultrasonic bath (B2500A-DTH; VWR International, Radnor, PA) for 10 min at 46°C and a frequency of 42 kHz to yield a homogenous size distribution. The resultant suspension had a lipid concentration of 10 mg/mL and an average vesicular size of 131.9 ± 1.1 nm (Fig. S1).

Surface tension measurement

Dynamic surface tensions of lipid vesicle adsorption were determined with CDS (40). CDS uses the air-water surface of a sessile drop (~10 μL in volume, ~3 mm in diameter, and ~0.2 cm^2 in surface area) to accommodate the adsorbed film. The droplet is "constrained" on a carefully machined pedestal that uses a knife-sharp edge to ensure a leak-proof environment. The dynamic surface tension was determined in real-time using axisymmetric drop shape analysis (ADSA) (42). One common artifact of studying lipid adsorption using droplet-based methods is that the adsorbed lipid films are spontaneously compressed because of droplet evaporation over time. This artifact was eliminated by maintaining a constant drop volume during the experiment, using a feedback control system called closed-loop ADSA (43). All measurements were carried out at 37 ± 0.1°C.

Film formation

The DPPC films at the air-water surface were formed with three different protocols (i.e., adsorption of DPPC vesicles (Protocol 1), spreading of DPPC vesicles (Protocol 2), and spreading of the DPPC monolayer (Protocol 3), respectively). As illustrated in Fig. 1, in Protocol 1, adsorption of DPPC vesicles was studied by injecting 4 μL DPPC stock suspension into a 16-μL buffer droplet (i.e., at a final DPPC concentration of 2 mg/mL). The dynamic surface tension was studied for 1 h with the drop volume controlled using closed-loop ADSA. In Protocol 2, a small amount of DPPC stock suspension (10 mg/mL) was spread onto a 12 μL buffer droplet. In Protocol 3, a small amount of DPPC dissolved in chloroform (1 mg/mL) was spread onto a 15-μL buffer droplet. For both Protocols 2 and 3, the dynamic surface tension was studied for 2 min, after which there was no significant change in the surface tension.

AFM imaging

The DPPC monolayer was Langmuir-Blodgett transferred from the droplet surface by lifting a small piece of freshly peeled mica sheet across the air-water interface of the droplet at a rate of 1 mm/min. For adsorbed DPPC films or DPPC films spread from the aqueous suspension (Protocols 1 and 2), before the Langmuir-Blodgett transfer, vesicles in the droplet were displaced with buffer using a subphase replacement technique (44). The immobilized DPPC films were scanned using an Innova AFM (Bruker, Billerica, MA) in air in contact mode using a silicon nitride cantilever with a spring constant of 0.12 N/m and a tip radius of 2 nm. Image analysis was conducted with Nanoscope Analysis (ver1.5).

Modification of the Martini force field

CGMD simulations were performed using a modified Martini force field with GROMACS 4.5.5 (45). Because the well of the Lennard-Jones (LJ) 12-6 potential is deep and narrow, the Martini water yields an air-water surface tension value of only 32 mN/m, far below the actual surface tension of water at room temperature (i.e., 72 mN/m). To solve this problem, we adopted the Chiu-Scott-Jakobosson (CSJ) water model (46) based on the Morse potential to replace the original Martini water. The Morse potential $V_M(r)$ was only used for water-water interactions:

$$V_M(r) = \varepsilon_M \left[e^{\alpha\left(1-\frac{r}{R_0}\right)} - 2e^{1/2\alpha\left(1-\frac{r}{R_0}\right)} \right] \quad r < r_c. \qquad (1)$$

It was prepared as user-specified tables, according to the GROMACS format, in which $\varepsilon_M = 3.4$ KJ/mol, $\alpha = 7$, and $R_0 = 0.629$ nm were determined based on previous calibrations (46). For other nonbonded interactions, the shifted LJ 12-6 potential $V_{LJ}(r)$ and the shifted Coulomb potential $V_C(r)$ with a shift function $S(r)$ as follows:

$$V_{LJ}(r) = 4\varepsilon_{LJ}\left[\left(\frac{\sigma}{r}\right)^{12} - \left(\frac{\sigma}{r}\right)^{6}\right] + S_{LJ}(r) \quad r < r_c, \qquad (2)$$

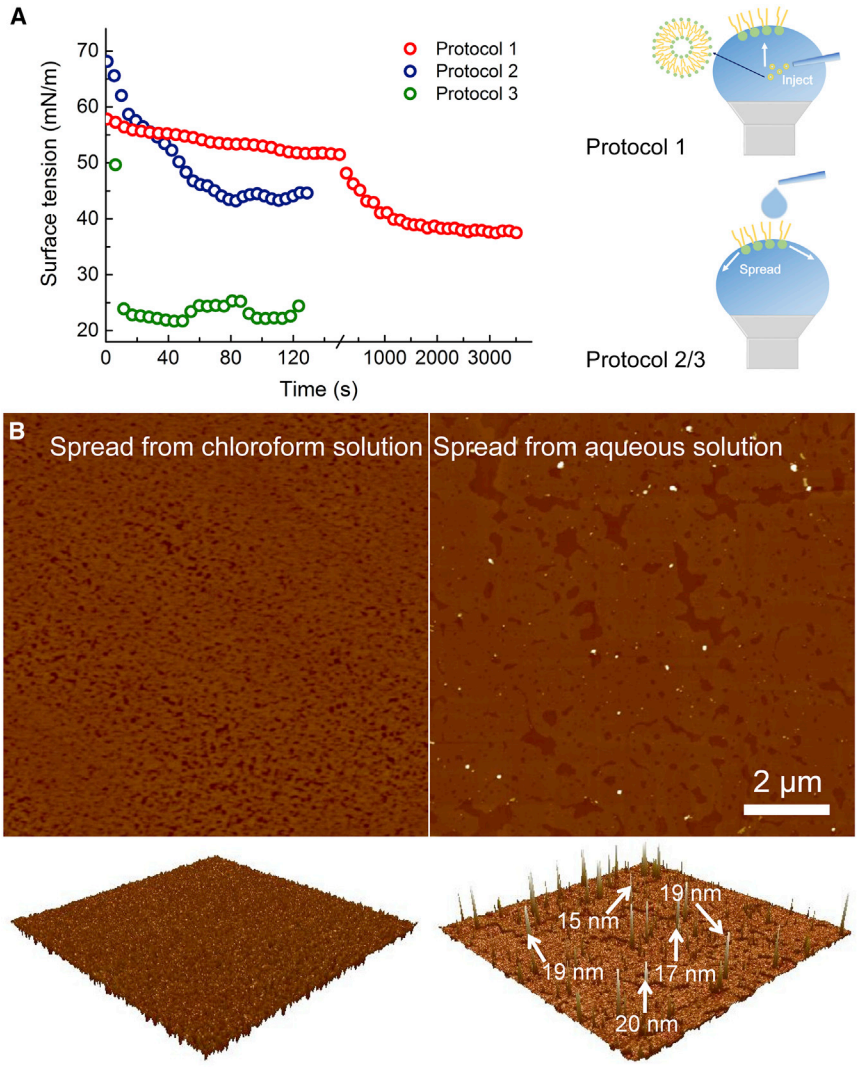

FIGURE 1 (*A*) Dynamic surface tension of DPPC determined with constrained drop surfactometry (CDS) at 37°C. Protocol 1 is as follows: injecting 4 μL 10 mg/mL DPPC suspension into a 16-μL buffer droplet. Protocol 2 is as follows: spreading 8 μL 10 mg/mL DPPC suspension onto a 12-μL buffer droplet. Protocol 3 is as follows: spreading 1 μL 1 mg/mL DPPC from chloroform onto a 15-μL water droplet. (*B*) Shown are AFM topographic images of the DPPC film (the second row shows the three-dimensional surface plot of the AFM images). All AFM images have the same scanning area of 10 × 10 μm. The images of DPPC spread from chloroform solution and aqueous solution have a z range of 5 and 20 nm, respectively. To see this figure in color, go online.

$$V_C(r) = \frac{q_i q_j}{4\pi\varepsilon_C} + S_C(r) \quad r < r_c, \tag{3}$$

$$S(r) = \begin{cases} C & r < r_1 \\ \frac{A}{3}(r - r_1)^3 + \frac{B}{4}(r - r_1)^4 + C & r_1 < r < r_c \end{cases}, \tag{4}$$

$$A = \left(-3E'(r_c) + (r_c - r_1)E''(r_c)\right)/(r_c - r_1)^2, \tag{5}$$

$$B = \left(3E'(r_c) - (r_c - r_1)E''(r_c)\right)/(r_c - r_1)^3, \tag{6}$$

$$C = -E(r_c) + \frac{1}{2}(r_c - r_1)E'(r_c) - \frac{1}{12}(r_c - r_1)^2 E''(r_c), \tag{7}$$

were adopted and tabulated in these simulations. The parameters, ε_{LJ}, σ, and q, followed the standard parameterization of the original Martini force field (62). The modified Martini force field was validated by directly comparing with experimentally determined DPPC compression isotherms at 37°C (53,54,63), as shown in Figs. S2 and S3.

MD simulations

Because of adoption of the CSJ water model, the temperature boundary conditions were set using the Nose-Hoover algorithm, and the pressure boundary conditions were set using the Parrinello-Rahman pressure coupling method. For temperature coupling, the water molecules and DPPC molecules were independently coupled with the relaxation time τ_T of 0.2 and 1.0 ps, respectively. The reference temperature was set at 310° K. For pressure coupling, semi-isotropic pressure coupling was used with the relaxation time τ_p of 2.0 ps and the compressibility of 5 e^{-6} bar^{-1} (47). The time step of all simulations was set at 5 fs. The standard cutoffs r_1 and r_c for the Martini force field were used. The LJ potential was shifted to zero between 0.9 and 1.2 nm, and the Coulomb potential was shifted to zero between 0 and 1.2 nm, with a relative dielectric constant ε_C of 15. The cutoff of the Morse potential was 1.6 nm. The nonbonding pair list was updated every five steps with the neighboring search cutoff of 1.6 nm. More details about the molecular dynamics (MD) simulations and the simulation files (Data S1) can be found in the Supporting Materials and Methods.

RESULTS AND DISCUSSION

Experimental measurements of the surface tension and morphology of DPPC films

Measurements of the surface tension of adsorbed and spread films were performed through three protocols (Fig. 1 *A*) with each measurement repeated for three times at 37°C (Figs. S4–S6). By injecting DPPC vesicles into the droplet (Protocol 1), the air-water surface tension decreases to a stable value of 41 mN/m after 30 min. For the case of spreading DPPC vesicles onto the droplet (Protocol 2), the surface tension shows more rapid reduction, indicating faster adsorption by eliminating the diffusion barrier. After only 80 s, a stable value close to that of the Protocol 1 is achieved. When spreading DPPC dissolved in the organic solvent (Protocol 3), the surface tension quickly drops to a stable value of 22 mN/m within 10 s. This value is close to the equilibrium surface tension between alkanes and water, indicating that the air-water surface is covered with alkane chains facing the air side.

As summarized in Table 1, DPPC vesicles both adsorbed and spread onto the air-water surface result in an equilibrium surface tension of 41 mN/m at 37°C. This value is close to that obtained with the micropipette technique (28) but significantly lower than that obtained with various bubble methods (26,27). Nevertheless, it is found that only the DPPC monolayer spread from organic solvent is able to reach the intrinsic equilibrium surface tension of the phospholipid monolayer (i.e., ~22 mN/m). AFM images (Fig. 1 *B*) show that the DPPC monolayer spread from organic solvent shows a closely packed homogeneous structure. However, the adsorbed DPPC film from aqueous suspension shows a loosely packed heterogeneous structure with protrusions between 15 and 20 nm in height (Fig. S7). Given the height of one DPPC bilayer at ~4–5 nm (48,49), these protrusions most likely represent three to four stacks of DPPC bilayers.

Adsorption of DPPC micelles and bilayers to a clean air-water surface

When immersed in the aqueous phase, DPPC molecules self-assemble into a variety of well-defined structures, such as micelles, bilayers, and vesicles due to hydrophobic interactions (Fig. 2 *A*) (50,51). We first simulate the adsorption process of self-assembled micelles and bilayers. Fig. S8 shows the setup and time evolution of the adsorption simulation. After dissolved in water, DPPC monomers quickly cluster into micelles that fuse with each other and grow further into larger planer structures (i.e., bilayers). Once adsorbed at the air-water surface, both the DPPC micelles and bilayers transform into a monolayer that covers the surface (Fig. 2, *B* and *C*). It should be noted that the DPPC micelles and bilayers simulated here contain unstable open edges. In comparison with closed vesicles, these unclosed structures can be only considered as intermediate self-assembled structures when studying the adsorption of spontaneously assembled DPPC aggregates in these MD simulations.

When contacting the surface, micelles break up and expose its hydrophobic interiors to the air side (Fig. 2 *B*). Different from micelles, bilayers undergo a more complicated and longer transformation process (Fig. 2 *C*). Note that the edge of the bilayer always first contacts the surface to create a connection between the bilayer and the surface. Once the connection is established, the bilayer splits into two leaflets that spread and transform into a steady monolayer at the air-water surface.

To analyze such structural transformations of the DPPC micelle and bilayer at the air-water surface, we establish the correlations between the phospholipids in the aqueous phase and those at the air-water surface by examining their free energies using established theories (13,14,52). Here, the energetic driving forces for lipid adsorption are attributed to the following three sources (Figs. S9 and S10). The first source is the free energy change of the phospholipids at the lipid-water surface, where a high energy state in the aqueous phase can drive the adsorption of micelles and bilayers to form a flat monolayer at the air-water surface. The second source is the surface energy change caused by creating an air-oil surface to replace the air-water surface, which drives spreading of the lipid molecules at the surface. The third source is the bending energy cost for establishing the connection between the bilayer and the monolayer. As shown in Fig. 2 *C*, the bilayer tends to adsorb vertically rather than parallelly to the surface to reduce the energy cost by minimizing the angle between the bilayer and the surface.

TABLE 1 Comparison of the Equilibrium Surface Tensions of Adsorbed and Spread DPPC Films at the Air-Water Surface at 37°C, Obtained with Various Experimental Methods

Method	Solute/Solvent	Surface Tension (mN/m)
CDS	Vesicle (132 nm)/PBS	41
CDS	Monomer/Chloroform	22
Bubble profile tensiometry (26)	Vesicle (80 nm)/HEPES	55
Pulsating bubble (27)	Vesicle/PBS	53
Micropipette technique (28)	Vesicle (100–150 nm)/PBS	39

Adsorption of DPPC micelles and bilayers to a pre-existing DPPC monolayer

By placing the DPPC molecules at the air-water surface as well as in the bulk phase simultaneously, we now study how the self-assembled DPPC micelles and bilayers adsorb to a loosely packed pre-existing monolayer (Fig. 3 *A*). As shown in Fig. 3 *B*, the surface tension of the DPPC film formed by the adsorption of micelles or bilayers reaches

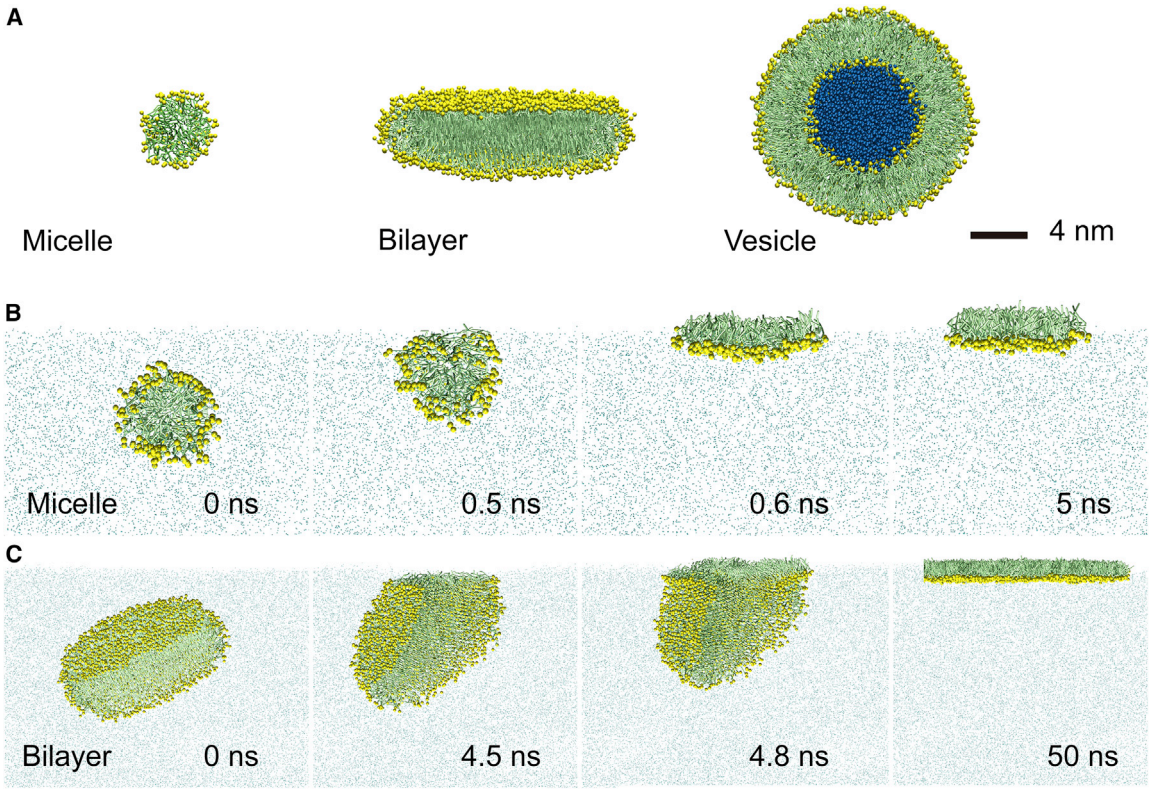

FIGURE 2 Sectional view of the different self-assembled DPPC structures (*A*) and the structural transformation of the DPPC micelle (*B*) and the DPPC bilayer (*C*) at the clean air-water interface. Note that, for clarity, the unclosed lamellar bilayer structure with the curved edge is defined as a bilayer, and the closed bilayer containing the interior water is defined as a vesicle. The DPPC molecules form a stable monolayer at the air-water surface after adsorption from the micelle and the bilayer. The polar moieties of DPPC are presented as yellow spheres. The hydrocarbon tails are shown as lime sticks. The water beads are shown as blue dots. The interior water beads within the vesicle are shown as blue spheres, for clarity. To see this figure in color, go online.

equilibrium at 30 mN/m, implying that the adsorbed DPPC molecules are closely packed at the interface.

The adsorption process is illustrated in Fig. 3, *C–E*. The actual adsorption behavior depends on the initial lipid density of the monolayer and the length of the bilayer. For a low-density monolayer (0.68 nm^2/molecule, Fig. 3 *C*), a short bilayer undergoes an adsorption process similar to adsorption to the clean air-water surface. The bilayer completely transforms to the flat monolayer, thus increasing the monolayer density to 0.48 nm^2/molecule. This molecular area corresponds to a compacted DPPC monolayer in the tilted condensed phase (53,54). For the same low-density monolayer (Fig. 3 *D*), a longer bilayer tends to bend and fold into a closed semivesicle to eliminate the hydrophobic effect at the edge of the bilayer. This structure is analogous to what Baoukina et al. reported on the transformation of an extruded bilayer into a semivesicle (55). They found that such a transformation only occurred when the bilayer perimeter exceeded a certain value, in which the hydrophobic energy of the open edge overcomes the bending energy to promote the folding of the bilayer. We have also found that a short bilayer, limited by its perimeter, can only protrude from the monolayer to the air phase to reduce the hydrophobic effect of its open edge (Fig. 3 *E*).

Adsorption of DPPC vesicles to a clean air-water surface

When the perimeter of the bilayer edge is large enough to provide a sufficiently large line energy to overcome its bending energy, the bilayer spontaneously curves into a closed spherical vesicle in water (Fig. S11) (2,56). Adsorption of lipid vesicles onto a surface is a classical model to investigate phospholipid adsorption (4). By depositing a vesicle onto a hydrophobic substrate, our simulations reveal that the vesicle unzips at the substrate and completely transforms into a monolayer (Fig. S12). These simulation results are consistent with existing experimental and computational observations on the adsorption of the phospholipid vesicle onto an alkyl-coated substrate (4,57).

When a vesicle adsorbs to the air-water surface, its outer leaflet first unzips and exposes its inner leaflet to air (Fig. 4 *A*). Then the outer leaflet spreads and transforms into a monolayer along the surface, whereas the inner leaflet enters the air phase to reduce the contact angle between the monolayer and the vesicle. Unlike spreading on a solid surface, spreading at the air-water surface is halted over time, which leaves a large portion of the air-water surface uncovered by the lipids (Fig. 4 *B* versus

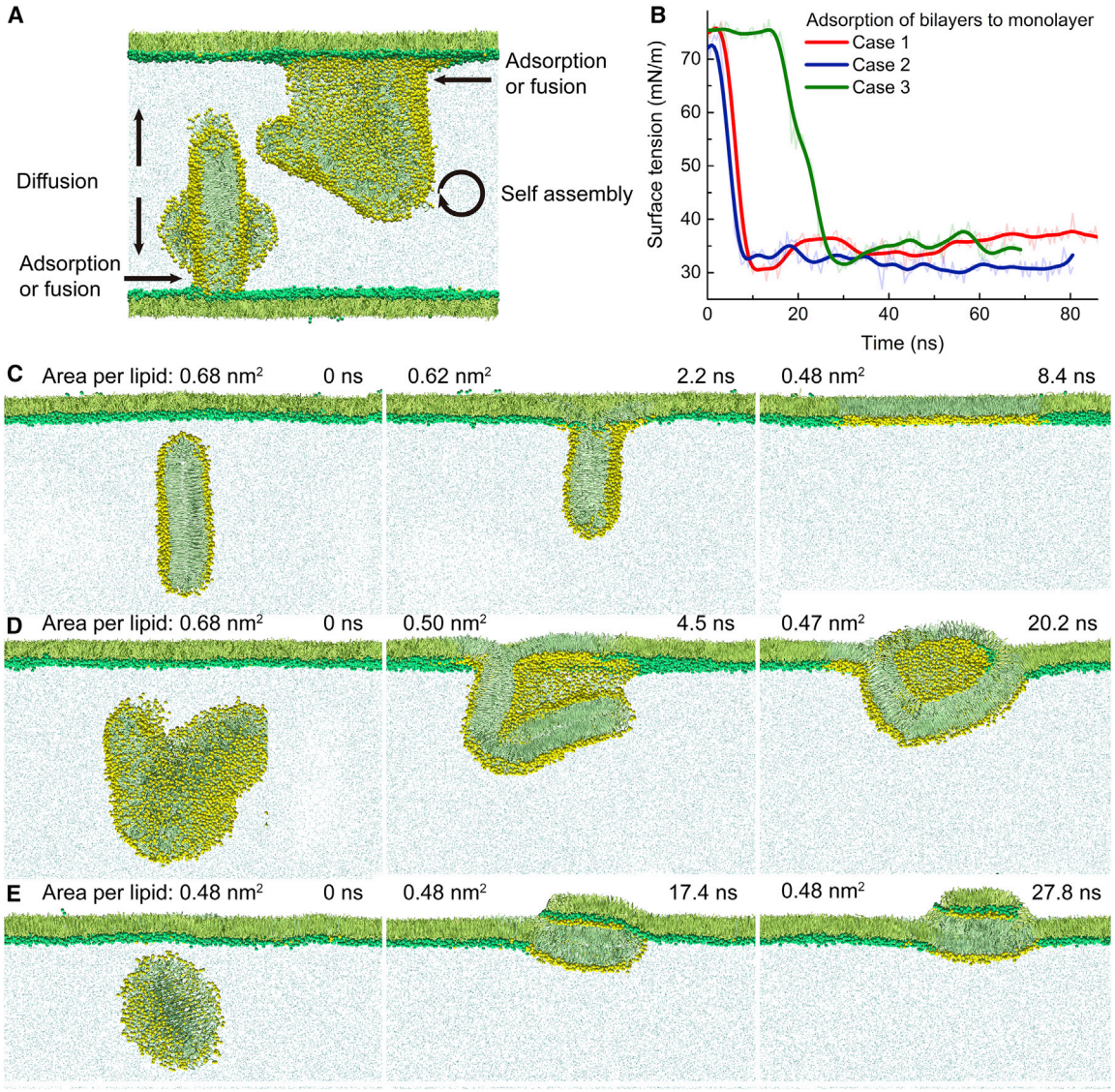

FIGURE 3 Adsorption of DPPC micelles and bilayers to the existing DPPC monolayer. (*A*) Shown is a schematic representation for the simulation system of the adsorption of the assembled micelles and bilayers to the sparse monolayer (0.7 nm^2). The polar moieties of DPPC at the surface were presented as green spheres, and the hydrocarbon tails were shown as green sticks. (*B*) Dynamic surface tension of the DPPC film were formed by the adsorption of the assembled micelles and bilayers. Three independent runs were performed to obtain the kinetics of the surface tension. (*C–E*) Snapshots for the fusion process of the assembly bilayers to the DPPC monolayer varied with the initial lipid density of the monolayer and the length of the bilayer. To see this figure in color, go online.

Fig. S12 *B*). Consequently, the inner leaflet of the vesicle is reserved to form an elliptical inverted micelle attaching to the spread monolayer. These inverted micelles can move freely along the monolayer (Fig. 4 *B*), probably coalescing with each other to form the large protrusions found by AFM (Fig. 1 *B*).

Because only one leaflet of the vesicle is capable of unzipping and spreading at the air-water surface, the capacity of adsorbed vesicles in reducing the dynamic surface tension is expected to be significantly lower than that of spread molecules. The inverted micelle attached to the interfacial monolayer increases its local curvature and leads to a weaker tail-tail interaction than that of a flat monolayer, thus increasing the surface tension. Besides, the inverted micelle will expand the area of the headgroups of the attached outer layer to weaken the interaction within the headgroups. The loosely packed headgroups also lead more hydrophobic tails to expose to the surrounding water and thus provide a higher hydrophobic energy to increase the surface tension. As shown in Fig. 5, in comparison with a spread monolayer via organic solvents, the adsorbed film has a much higher surface tension. These simulation results are in good agreement with our experimental observations (Fig. 1; Table 1).

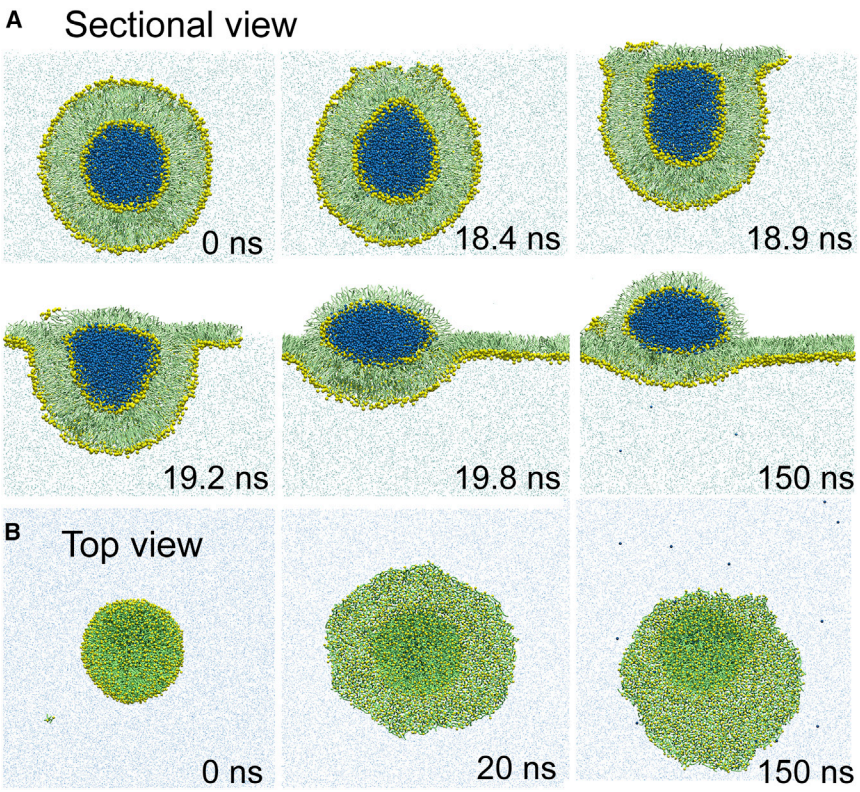

FIGURE 4 Snapshots for the structural transformation of the DPPC vesicle at the clean air-water surface from the sectional view (*A*) and the top view (*B*). Snapshots for the structural transformation of the DPPC vesicle at a hydrophobic solid surface are shown in Fig. S12. The DPPC molecules of the outer leaflet of the vesicle cannot spread at the air-water interface within hundreds of nanoseconds after they transform to a monolayer at the surface (Fig. S13). To see this figure in color, go online.

Adsorption of DPPC vesicle to a pre-existing monolayer

By placing a vesicle between two monolayers, we investigate the adsorption of the DPPC vesicle to a pre-existing monolayer (Fig. 6 *A*). As indicated in the dynamic surface tension curve of the adsorbed film (Fig. 6 *B*), the vesicle can adsorb to the pre-existing monolayer independent of the initial lipid density of the monolayer. The adsorbed vesicles reduce the surface tension of the monolayer to 55 mN/m, which is significantly higher than the equilibrium surface tension of the DPPC film formed by the adsorption of micelles and bilayers (Fig. 3 *B*). As shown in the dynamic process of the vesicle adsorption (Fig. 6 *C*), similar to vesicle adsorption to the clean air-water surface (Fig. 4), the inner leaflet of the vesicle remains intact and forms an inverted micelle facing the air side, thus not contributing to surface tension reduction.

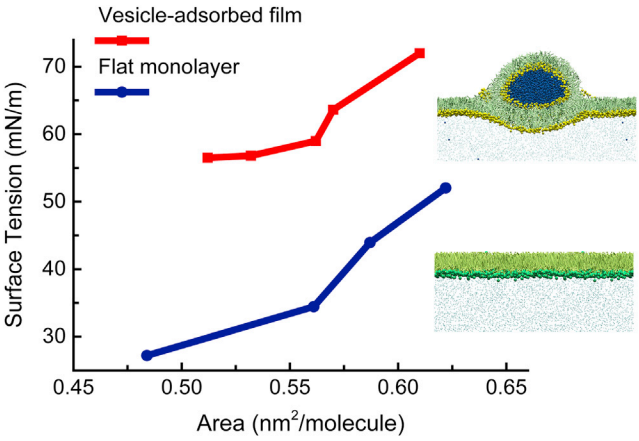

FIGURE 5 Surface tension-area isotherms of the vesicle-adsorbed and molecule-spread films. When calculating the molecular area of the vesicle-adsorbed film, only those lipid molecules spread at the flat air-water surface (excluding those lipid molecules composed of the inverted micelle) were counted in MD simulations. To see this figure in color, go online.

Our simulations provide, to our knowledge, novel insights into the adsorption mechanisms of pulmonary surfactants and other lipids. Different from DPPC vesicles, natural pulmonary surfactant undergoes a fast adsorption process at the air-water surface and achieves an equilibrium surface tension around 22 mN/m (21,23,58). Natural pulmonary surfactant consists of multiple lipid components, with DPPC being the major phospholipid component, and surfactant-associated proteins (8,19). Both experimental and simulation results show that adsorbed films from pure DPPC vesicles have a high surface tension up to 40 mN/m. Our CGMD simulations revealed that this high surface tension was caused by the curvature effect of inverted micelles composed of nonspread lipid molecules (Figs. 5 and 6). Hence, the low surface tension of adsorbed pulmonary surfactant can only be achieved with other surfactant components that help reduce or eliminate the local curvature effect. Unsaturated phospholipids and hydrophobic surfactant proteins can lower the energy barrier of the pore formation

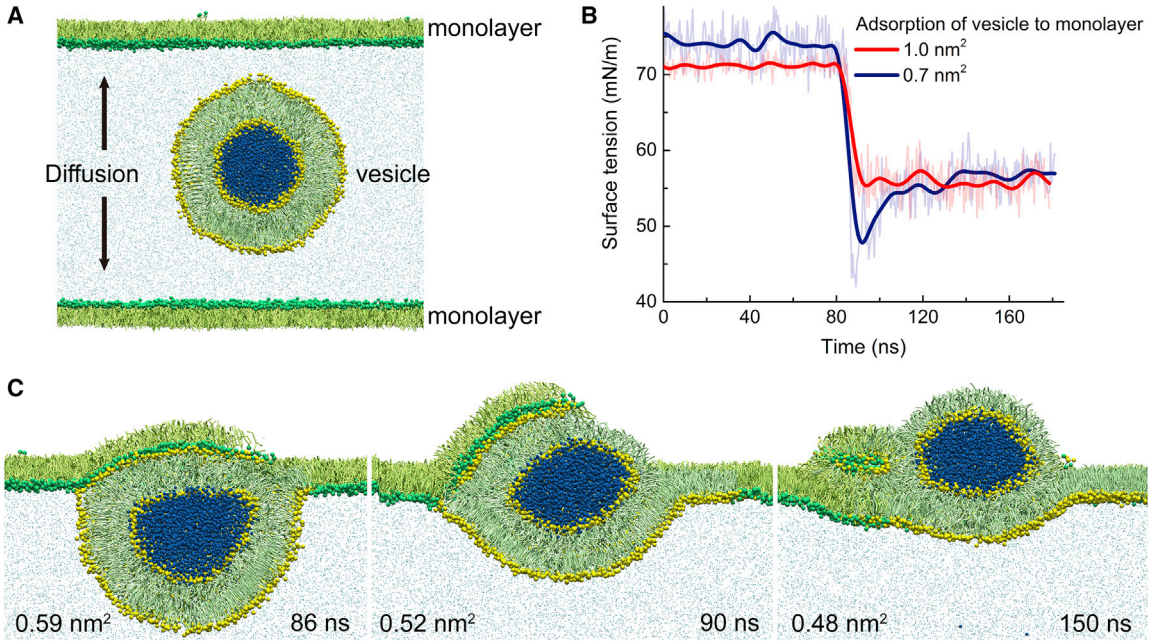

FIGURE 6 Adsorption of the vesicle to the existing DPPC monolayer. (*A*) Shown is a schematic representation for the simulation system of the adsorption of the vesicle to the sparse monolayer. (*B*) Shown is the dynamic surface tension of the DPPC film adsorbed with the DPPC vesicle. The molecular area of the initial monolayer was set to 1.0 and 0.7 nm^2. (*C*) Shown are snapshots for the fusion process of the vesicle to the sparse DPPC monolayer (0.7 nm^2). To see this figure in color, go online.

of a vesicle (59,60), which may contribute to the breakup of the inverted micelle and thus help eliminate the local curvature effect.

CONCLUSIONS

Using DPPC as a model system, we studied the adsorption of phospholipids at the air-water surface. Both experimental observations and CGMD simulations demonstrated that the adsorbed DPPC film from vesicles exhibits a much higher equilibrium surface tension than spread film from the organic solvent. Our simulations showed that only the outer leaflet of the vesicle can unzip and spread at the air-water surface, whereas the inner leaflet remains intact as an inverted micelle attaching to the monolayer. The inverted micelle increases the local curvature of the monolayer, thus leading to a loosely packed monolayer at the air-water surface and hence a higher surface tension. These findings provide novel insights into the mechanism of the phospholipid and pulmonary surfactant adsorption.

SUPPORTING MATERIAL

Supporting Material can be found online at https://doi.org/10.1016/j.bpj.2019.08.022.

AUTHOR CONTRIBUTIONS

Y.Y.Z. and G.H. designed the research. X.B. performed the simulations. L.X. and J.Y.T. performed the experiments. X.B., L.X., Y.Y.Z., and G.H. analyzed and interpreted the data. X.B., Y.Y.Z., and G.H. wrote the manuscript. X.B. and L.X. contributed equally to this work.

ACKNOWLEDGMENTS

This work was supported by Natural Science Foundation of China (11832017, 11572334, 91543125), the Chinese Academy of Sciences Key Research Program of Frontier Sciences (QYZDB-SSW-JSC036), and the Chinese Academy of Sciences Strategic Priority Research Program (XDB22040403) to G.H. and National Science Foundation (CBET-1604119) and the Hawai'i Community Foundation (18ADVC-90802) to Y.Y.Z. The MD simulations were performed on TianHe-1(A) at the National Supercomputing Center in Tianjin.

SUPPORTING CITATIONS

Reference (61) appears in the Supporting Material.

REFERENCES

1. Seifert, U. 1997. Configurations of fluid membranes and vesicles. *Adv. Phys.* 46:13–137.
2. Huang, C., D. Quinn, …, K. J. Hsia. 2017. Formation and size distribution of self-assembled vesicles. *Proc. Natl. Acad. Sci. USA.* 114:2910–2915.
3. Richter, R. P., R. Bérat, and A. R. Brisson. 2006. Formation of solid-supported lipid bilayers: an integrated view. *Langmuir.* 22:3497–3505.
4. Jass, J., T. Tjärnhage, and G. Puu. 2000. From liposomes to supported, planar bilayer structures on hydrophilic and hydrophobic surfaces: an atomic force microscopy study. *Biophys. J.* 79:3153–3163.
5. Seifert, U., and R. Lipowsky. 1990. Adhesion of vesicles. *Phys. Rev. A.* 42:4768–4771.

6. Chan, Y. H., and S. G. Boxer. 2007. Model membrane systems and their applications. *Curr. Opin. Chem. Biol.* 11:581–587.
7. Steinem, C., A. Janshoff, …, H. J. Galla. 1996. Impedance analysis of supported lipid bilayer membranes: a scrutiny of different preparation techniques. *Biochim. Biophys. Acta.* 1279:169–180.
8. Zuo, Y. Y., R. A. Veldhuizen, …, F. Possmayer. 2008. Current perspectives in pulmonary surfactant–inhibition, enhancement and evaluation. *Biochim. Biophys. Acta.* 1778:1947–1977.
9. Kulovesi, P., J. Telenius, …, J. M. Holopainen. 2010. Molecular organization of the tear fluid lipid layer. *Biophys. J.* 99:2559–2567.
10. Lugea, A., A. Salas, …, J. R. Malagelada. 2000. Surface hydrophobicity of the rat colonic mucosa is a defensive barrier against macromolecules and toxins. *Gut.* 46:515–521.
11. Hills, B. A. 2002. Surface-active phospholipid: a Pandora's box of clinical applications. Part II. Barrier and lubricating properties. *Intern. Med. J.* 32:242–251.
12. Schindler, H. 1979. Exchange and interactions between lipid layers at the surface of a liposome solution. *Biochim. Biophys. Acta.* 555:316–336.
13. Jähnig, F. 1984. Lipid exchange between membranes. *Biophys. J.* 46:687–694.
14. Feng, S. S. 1999. Interpretation of mechanochemical properties of lipid bilayer vesicles from the equation of state or pressure-area measurement of the monolayer at the air-water or oil-water interface. *Langmuir.* 15:998–1010.
15. Marsh, D. 1996. Lateral pressure in membranes. *Biochim. Biophys. Acta.* 1286:183–223.
16. Veldhuizen, R., K. Nag, …, F. Possmayer. 1998. The role of lipids in pulmonary surfactant. *Biochim. Biophys. Acta.* 1408:90–108.
17. Rugonyi, S., S. C. Biswas, and S. B. Hall. 2008. The biophysical function of pulmonary surfactant. *Respir. Physiol. Neurobiol.* 163:244–255.
18. Zasadzinski, J. A., J. Ding, …, A. J. Waring. 2001. The physics and physiology of lung surfactants. *Curr. Opin. Colloid Interface Sci.* 6:506–513.
19. Pérez-Gil, J. 2008. Structure of pulmonary surfactant membranes and films: the role of proteins and lipid-protein interactions. *Biochim. Biophys. Acta.* 1778:1676–1695.
20. Stenger, P. C., G. Wu, …, J. A. Zasadzinski. 2009. X-ray diffraction and reflectivity validation of the depletion attraction in the competitive adsorption of lung surfactant and albumin. *Biophys. J.* 97:777–786.
21. Walters, R. W., R. R. Jenq, and S. B. Hall. 2000. Distinct steps in the adsorption of pulmonary surfactant to an air-liquid interface. *Biophys. J.* 78:257–266.
22. Zuo, Y. Y., R. Gitiafroz, …, A. W. Neumann. 2005. Effect of humidity on the adsorption kinetics of lung surfactant at air-water interfaces. *Langmuir.* 21:10593–10601.
23. Notter, R. H., J. N. Finkelstein, and R. D. Taubold. 1983. Comparative adsorption of natural lung surfactant, extracted phospholipids, and artificial phospholipid mixtures to the air-water interface. *Chem. Phys. Lipids.* 33:67–80.
24. Launoissurpas, M. A., T. Ivanova, …, G. Georgiev. 1992. Behavior of pure and mixed Dppc liposomes spread or adsorbed at the air-water-interface. *Colloid Polym. Sci.* 270:901–911.
25. Wen, X., and E. I. Franses. 2001. Role of subsurface particulates on the dynamic adsorption of dipalmitoylphosphatidylcholine at the air/water interface. *Langmuir.* 17:3194–3201.
26. Nguyen, P. N., G. Waton, …, M. P. Krafft. 2013. Behavior of an adsorbed phospholipid monolayer submitted to prolonged periodical surface density variations. *Angew. Chem. Int.Engl.* 52:6404–6408.
27. Chang, C. H., K. A. Coltharp, …, E. I. Franses. 1996. Surface tension measurements with the pulsating bubble method. *Colloids Surf. A Physicochem. Eng. Asp.* 114:185–197.
28. Lee, S., D. H. Kim, and D. Needham. 2001. Equilibrium and dynamic interfacial tension measurements at microscopic interfaces using a micropipet technique. 2. Dynamics of phospholipid monolayer formation and equilibrium tensions at the water-air interface. *Langmuir.* 17:5544–5550.
29. Kim, S. H., and E. I. Franses. 2005. New protocols for preparing dipalmitoylphosphatidylcholine dispersions and controlling surface tension and competitive adsorption with albumin at the air/aqueous interface. *Colloids Surf. B Biointerfaces.* 43:256–266.
30. Kim, S. H., Y. Park, …, E. I. Franses. 2008. Effect of buffer composition and preparation protocol on the dispersion stability and interfacial behavior of aqueous DPPC dispersions. *Colloids Surf. B Biointerfaces.* 67:253–260.
31. Nguyen, P. N., T. T. Trinh Dang, …, M. P. Krafft. 2011. A nonpolar, nonamphiphilic molecule can accelerate adsorption of phospholipids and lower their surface tension at the air/water interface. *ChemPhysChem.* 12:2646–2652.
32. Pinazo, A., X. Y. Wen, …, E. I. Franses. 2002. Comparison of DLPC and DPPC in controlling the dynamic adsorption and surface tension of their aqueous dispersions. *Langmuir.* 18:8888–8896.
33. Marrink, S. J., and D. P. Tieleman. 2013. Perspective on the Martini model. *Chem. Soc. Rev.* 42:6801–6822.
34. Hu, G., B. Jiao, …, Y. Y. Zuo. 2013. Physicochemical properties of nanoparticles regulate translocation across pulmonary surfactant monolayer and formation of lipoprotein corona. *ACS Nano.* 7:10525–10533.
35. Hu, Q., X. Bai, …, Y. Y. Zuo. 2017. Unveiling the molecular structure of pulmonary surfactant corona on nanoparticles. *ACS Nano.* 11:6832–6842.
36. Yue, T., and X. Zhang. 2013. Molecular modeling of the pathways of vesicle–membrane interaction. *Soft Matter.* 9:559–569.
37. Shi, X., and F. Tian. 2018. Multiscale modeling and simulation of nanocarriers delivery through biological barriers—a review. *Adv. Theory Simul.* 2:1800105.
38. Baoukina, S., L. Monticelli, …, D. P. Tieleman. 2007. The molecular mechanism of monolayer-bilayer transformations of lung surfactant from molecular dynamics simulations. *Biophys. J.* 93:3775–3782.
39. Baoukina, S., and D. P. Tieleman. 2011. Lung surfactant protein SP-B promotes formation of bilayer reservoirs from monolayer and lipid transfer between the interface and subphase. *Biophys. J.* 100:1678–1687.
40. Valle, R. P., T. Wu, and Y. Y. Zuo. 2015. Biophysical influence of airborne carbon nanomaterials on natural pulmonary surfactant. *ACS Nano.* 9:5413–5421.
41. Blume, A. 1983. Apparent molar heat-capacities of phospholipids in aqueous dispersion - effects of chain-length and head group-structure. *Biochemistry.* 22:5436–5442.
42. Yang, J., K. Yu, and Y. Y. Zuo. 2017. Accuracy of axisymmetric drop shape analysis in determining surface and interfacial tensions. *Langmuir.* 33:8914–8923.
43. Yu, K., J. Yang, and Y. Y. Zuo. 2016. Automated droplet manipulation using closed-loop axisymmetric drop shape analysis. *Langmuir.* 32:4820–4826.
44. Yang, Y., L. Xu, …, Y. Y. Zuo. 2018. Aggregation state of metal-based nanomaterials at the pulmonary surfactant film determines biophysical inhibition. *Environ. Sci. Technol.* 52:8920–8929.
45. Hess, B., C. Kutzner, …, E. Lindahl. 2008. GROMACS 4: algorithms for highly efficient, load-balanced, and scalable molecular simulation. *J. Chem. Theory Comput.* 4:435–447.
46. Chiu, S. W., H. L. Scott, and E. Jakobsson. 2010. A coarse-grained model based on Morse potential for water and n-alkanes. *J. Chem. Theory Comput.* 6:851–863.
47. Duncan, S. L., and R. G. Larson. 2008. Comparing experimental and simulated pressure-area isotherms for DPPC. *Biophys. J.* 94:2965–2986.
48. von Nahmen, A., M. Schenk, …, M. Amrein. 1997. The structure of a model pulmonary surfactant as revealed by scanning force microscopy. *Biophys. J.* 72:463–469.
49. Zuo, Y. Y., E. Keating, …, F. Possmayer. 2008. Atomic force microscopy studies of functional and dysfunctional pulmonary surfactant

films. I. Micro- and nanostructures of functional pulmonary surfactant films and the effect of SP-A. *Biophys. J.* 94:3549–3564.

50. Israelachvili, J. N., D. J. Mitchell, and B. W. Ninham. 1976. Theory of self-assembly of hydrocarbon amphiphiles into micelles and bilayers. *J. Chem. Soc., Faraday Trans. II.* 72:1525–1568.

51. Israelachvili, J. N., D. J. Mitchell, and B. W. Ninham. 1977. Theory of self-assembly of lipid bilayers and vesicles. *Biochim. Biophys. Acta.* 470:185–201.

52. Jähnig, F. 1996. What is the surface tension of a lipid bilayer membrane? *Biophys. J.* 71:1348–1349.

53. Zuo, Y. Y., R. Chen, …, A. W. Neumann. 2016. Phase transitions in dipalmitoylphosphatidylcholine monolayers. *Langmuir.* 32:8501–8506.

54. Xu, L., and Y. Y. Zuo. 2018. Reversible phase transitions in the phospholipid monolayer. *Langmuir.* 34:8694–8700.

55. Baoukina, S., L. Monticelli, …, D. P. Tieleman. 2008. The molecular mechanism of lipid monolayer collapse. *Proc. Natl. Acad. Sci. USA.* 105:10803–10808.

56. Helfrich, W. 1973. Elastic properties of lipid bilayers: theory and possible experiments. *Z. Naturforsch. C.* 28:693–703.

57. Mannelli, I., F. Sagués, …, R. Reigada. 2016. Lipid vesicle interaction with hydrophobic surfaces: a coarse-grained molecular dynamics study. *Langmuir.* 32:12632–12640.

58. Wang, Z., S. B. Hall, and R. H. Notter. 1996. Roles of different hydrophobic constituents in the adsorption of pulmonary surfactant. *J. Lipid Res.* 37:790–798.

59. Marrink, S. J., A. H. de Vries, and D. P. Tieleman. 2009. Lipids on the move: simulations of membrane pores, domains, stalks and curves. *Biochim. Biophys. Acta.* 1788:149–168.

60. Parra, E., A. Alcaraz, …, J. Pérez-Gil. 2013. Hydrophobic pulmonary surfactant proteins SP-B and SP-C induce pore formation in planar lipid membranes: evidence for proteolipid pores. *Biophys. J.* 104:146–155.

61. Kaznessis, Y. N., S. Kim, and R. G. Larson. 2002. Simulations of zwitterionic and anionic phospholipid monolayers. *Biophys. J.* 82:1731–1742.

62. Marrink, S. J., H. J. Risselada, …, A. H. de Vries. 2007. The MARTINI force field: coarse grained model for biomolecular simulations. *J. Phys. Chem. B.* 111:7812–7824.

63. Baoukina, S., L. Monticelli, …, D. P. Tieleman. 2007. Pressure-area isotherm of a lipid monolayer from molecular dynamics simulations. *Langmuir.* 23:12617–12623.